Chinese Physics B

Tuning the particle size, physical properties, and photocatalytic activity of Ag_3PO_4 materials by changing Ag^+/PO_4^{3-} ratio

To cite this article before publication: Hung N. M. *et al* 2022 *Chinese Phys. B* in press https://doi.org/10.1088/1674-1056/ac84ce

Tuning the particle size, physical properties, and photocatalytic activity of Ag_3PO_4 materials by changing Ag^+/PO_4^{3-} ratio

Hung N. M.[1,3], Oanh L. T. M.[1,2*], Chung D. P.[2], Thang D. V.[1.3], Mai V. T.[1,4], Hang L. T.[1,5], Minh N. V.[1,2]

[1]*Center for Nano Science and Technology, Hanoi National University of Education, 136 Xuan Thuy Road, Cau Giay District, Hanoi 100000, Vietnam*

[2]*Department of Physics, Hanoi National University of Education, 136 Xuan Thuy Road, Cau Giay District, Hanoi 100000, Vietnam*

[3] *Hanoi University of Mining and Geology, Duc Thang ward, North Tu Liem District, Hanoi 100000, Vietnam*

[4]*Institute of Materials Science, Vietnam Academy of Science and Technology, 18 Hoang Quoc Viet, Hanoi 100000, Viet Nam*

[5] *Faculty of Basic Sciences, Hanoi University of Natural Resources and Environment, 41A Phu Dien Road, North Tu Liem, Hanoi 100000, Vietnam*

**Corresponding author email: lemaioanh@gmail.com*

Abstract This study demonstrated the influence of Ag^+/PO_4^{3-} ratio in precursor solution on the crystal structural formation, morphology, physical properties, and photocatalytic performance of Ag_3PO_4 photocatalyst fabricated by facile precipitation method from $AgNO_3$ and $Na_2HPO_4.12H_2O$. The material characterizations were investigated using X-ray diffraction (XRD), scanning electron microscopy (SEM), energy-dispersive X-ray spectroscopy (EDX), Brunauer-Emmett-Teller (BET) surface area, Fourier transform infrared (FTIR) absorption, Raman scattering, X-ray photoelectron spectroscopy (XPS), UV-vis absorption, and photoluminescence (PL). The results show that Ag_3PO_4 crystallizes better when the excess PO_4^{3-} content increases, the lattice parameters decrease slightly while the crystal diameter and the particle size increase. This change is also observed in the Raman scattering and FTIR spectra with the increase in the vibration frequency of the $[PO_4]$ group. The compression of the $[PO_4]$ unit was also confirmed in the XPS spectra with the shift of P 2p peaks toward to higher binding energy. The photocatalytic results showed that the samples synthesized from excess PO_4^{3-} solution exhibited higher photocatalytic performance comparing to sample with Ag^+/PO_4^{3-} ratio of 3:1. Sample prepared from the precursor solution with Ag^+/PO_4^{3-} ratio of 3:1.5 was optimal for RhB decomposition under both visible light and natural sunlight, completely decomposing RhB 10 ppm after 15 minutes of Xenon lamp irradiation and after 60 minutes under solar light irradiation. This is attributed to the high crystallinity, small particle size and low electron-hole recombination rate of sample.

Keywords: morphology, photocatalytic, Ag^+/PO_4^{3-} ratio, visible light

1. Introduction

Recently, among various photocatalysts, silver orthophosphate Ag_3PO_4 (APO) has emerged as a breakthrough in the field of visible light photocatalysis due to its small optical band gap of 2.43 eV, high quantum efficiency, and superior photooxidative capability [1, 2]. Since the formation of electron/hole pairs on the surface of APO particles plays an important role in the photocatalytic performance, many studies have been caried out with the aim of controlling the particle size or particle morphology to increase the specific surface area [3-6]. The studies showed that synthesis parameters such as the precipitating agents [7, 8], the ratios of starting materials [9, 10],

the concentraiton of the reaction catalysts [5, 11], the fabrication time [3, 4, 12], and pH conditions [13] greatly influence the size and morphology of the particles.

Although possessing great potential in the field of environmental remediation and renewable energy, APO has its own disadvantage of consuming a large amount of silver metal due to its wide use, leading to the increase of photocatalyst cost [4]. More importantly, during the photocatalytic activity, the Ag^+ ions in the APO lattice are susceptible to metalization upon receiving electrons, leading to undesirable and uncontrolled photocorrosion [14, 15]. As a result, the structure of the material is destroyed over time and the photocatalytic activity decreases. This has remained a challenge for researchers so far. Therefore, besides finding solutions to increase specific surface area, the researchers also focus on enhancing the structural stability of the materials through adjusting the ratio of Ag^+ and PO_4^{3-} [9, 16, 17] to find out the most stability structure. In addition, increasing the lifetime of the electron/hole pair to increase the photocatalytic efficiency has always been of interest to research through the creation of heterojunction between APO and other semiconductors [15, 18-21] as well as doping into APO with suitable ions [22-24].

The previous studies showed that the different concentrations of Ag^+ and PO_4^{3-} in starting solutions significantly affects the particle size and morphology, crystallinity, absorption capability and structure stability of Ag_3PO_3. Febiyanto used the precursors of $AgNO_3$ and $Na_2HPO_4.12H_2O$ with a given molar ratio of 3:1 and varied the concentration of both $AgNO_3$ and Na_2HPO_4 precursor solution. The result showed that Ag_3PO_3 prepared from the 1.0 M $AgNO_3$ and 0.33M $Na_2HPO_4.12H_2O_4$ solutions exhibited the highest photocatalytic activity [9]. The authors believed that the reason is due to the different concentrations in the reaction solution affecting the nucleation and crystal growth during the sample preparation. Still using $AgNO_3$ and Na_2HPO_4 with no change in mass and molar ratio in different samples but with varying concentrations of ammonia added, Febiyanto [17] found that a concentration of 0.05M ammonia was suitable for synthesis Ag_3PO_4 has the highest photocatalytic activity, increased 4.13 times compared to the Ag_3PO_4 prepared without the ammonia. This result was explained by the fact that the appropriate presence of ammonia successfully reduced the particle size and increased the homogeneity of the catalyst, in favor of the photocatalytic activity. Qin J. [16] when using $AgNO_3$ and $NH_4H_2PO_4$ as a starting materials found that the rich Ag^+ ion Ag_3PO_4 can form the surface plasmon resonance (SPR) of Ag nanoparticles to reduce the corrosion of Ag_3PO_4, thus enhancing the photocatalytic activity and stability (highest for sample with Ag^+/PO_4^{3-} ratio of 3:1). Afifah K. [10] used $AgNO_3$ and KH_2PO_4 as reactants and changed the Ag^+/PO_4^{3+} ratio by changing the KH_2PO_4 concentration in aqueous solution of 0.10 M, 0.15 M, 0.30 M, 0.45 M, and 0.60 M while keeping the same concentration and amount of $AgNO_3$ solution. The results show that the Ag_3PO_4 fabricated from 20 ml of 0.15 M KH_2PO_4 and 50 ml of 0.1 M $AgNO_3$ (Ag^+/PO_4^{3-} ratio of 3:1.8) exhibits superior photocatalytic activity. This is attributed to the small size of the mixture morphology of spheres and tetrahedra, high crystallinity and formation of defect sites.

Although the use of $Na_2HPO_4.12H_2O$ as a precursor has been studied, unfortunately, the effect of the Ag^+/PO_4^{3-} ratio on the photocatalytic performance of the material has not been reported. The objective of this study was to use excess $Na_2HPO_4.12H_2O$ as a source of phosphate ions with the hope that the excess of PO_4^{3-} would limit the aggregation of Ag^+ and thus prevent the metallization to Ag^o. As a result, APO nuclei would be easier to form and crystallize better. The

ratio of Ag^{+}/PO_4^{3-} was adjusted to 3:1; 3:1.5; 3:2 and 3:3. The study focused on the investigation of the variation of crystallinity, crystal structure, and other physical properties, and photocatalytic activity as a consequence of increasing excess PO_4^{3-} concentrations. In addition, to demonstrate the superior applicability of the fabricated APO, besides using visible light, the photocatalytic activity was also carried out under the irrasiation of natural sunlight at noon.

2. Materials and methods

2.1 Materials

The chemicals used in this work are silver nitrate ($AgNO_3$, Sigma-Aldrich, 99%) and disodium hydrogen phosphate 12-hydrate ($Na_2HPO_4.12H_2O$, Sigma-Aldrich, 99%). Rhodamine B ($C_{28}H_{31}ClN_2O_3$, Sigma-Aldrich, 95%) was used as an organic colorant in the photocatalytic test. These starting materials were used without further purification. The Xenon lamp (300W/220V) were used as the visible light source irradiation.

2.2 Synthesis of photocatalysts

Ag_3PO_4 materials were synthesized by a facile precipitation method. Firstly, 0.5096 g of $AgNO_3$ was dissolved in 150 ml of distilled water to achieve 0.02M Ag^{+} solution (solution A). In four separate beakers containing 50 ml, 75 ml, 100 ml and 150 ml of distilled water, dissolving 0.1420 g, 0.2129 g, 0.2839 g and 0.4259 g Na2HPO4.12H2O to obtain the 0.02 M PO_4^{3-} solution (solution B). With such amounts of starting materials, the adjusted Ag^{+}/PO_4^{3-} ratio was adjusted to be 3:1, 3:1.5, 3:2, 3:3. Next, the solution A was slowly dripped into the solution B to obtain a mixture of solution C. The solution C was magnetically stirred for 3 h at room temperature, a yellow precipitate was obtained. Filter and wash the precipitate 5 times with distilled water which was then dried at 100^{o}C to obtain yellow powder Ag_3PO_4.

For the convenience of description, different samples are named as Ag/P 3:1, Ag/P 3:1.5, Ag/P 3:2, and Ag/P 3:3 corresponding to Ag^{+}/PO_4^{3-} ratios of 3:1, 3:1.5, 3:2, and 3:3, respectively.

2.3 Characterization

Crystal structure of the samples was investigated using X-ray diffractometer (XRD, Brucker D8 Advance) with Cu Kα (λ = 1.54064 Å) radiation over Bragg angles ranging from 20° to 90°. Scanning electron microscope (SEM, JED-2300) equipped with energy dispersive X-ray spectroscopy (EDS) was used to study the morphology and elemental composition of the samples. The Brunauer-Emmett-Teller (BET) surface area was measured by a high-performance adsorption analyzer (Micromeritics 3Flex). FTIR/NIR spectrometer (Shimadzu IR Prestige-21) was used to carry out Fourier transform infrared spectra (FTIR) *of as-synthesized samples. Raman scattering spectra were conducted by a Raman microscope* (Horiba LabRam HR Evolution) using 532 nm laser beam as an excitation source. UV-vis diffuse reflectance spectra (DRS) were performed on a UV-vis spectrophotometer (Jasco V670). Furthermore, the surface element composition analysis of Ag_3PO_4 samples was studied using X-ray photoelectron spectroscopy with the energy resolution of 0.1 eV (XPS, Thermo Scientific Multilab-2000) using an Al Kα monochromatized source. Photoluminescence (PL) spectra were performed on a

fluorescence spectrophotometer (Nanolog Horiba iHR 550) using an excitation wavelength of 350 nm.

2.4 Photocatalytic activity test

In this study, 10ppm Rhodamine B (RhB) solution was used as a color indicator to evaluate the visible-light-driven photocatalytic performance of APO to decompose organic molecule. Xenon lamp (300W/220V) is used as the excitation visible light source. At the same time, natural sunlight was also used as a reference measurement.

Firstly, 0.06 g of APO was dissolved in 30 ml of distilled water then magnetically stirred for 30 min. Secondly, 30 ml of 20 ppm RhB solution was added to above solution (the final concentration of RhB solution for photocatalysis was 10 ppm). The mixture was magnetically stirred in a dark chamber for 30 min to reach adsorption-desorption equilibrium state. After dark stirring, the solution was illuminated under a Xenon lamp using a UV cut-off filter to investigate the visible-light-driven photocatalytic properties of the sample. The distance between Xenon lamp and the surface of RhB solution is 10 cm (illuminance of 23121 lux). After each 5 minutes (or 10 minutes), an amount of 4 ml of RhB solution was removed and centrifuged at 4000 rpm to remove APO powder. The concentration of RhB remaining in the solution at a time was assessed through the absorption spectrum of the solution. The absorption intensity of the characteristic absorption peak of RhB at 554 nm was used to determine the remaining content of RhB in the solution at a time by using a standard curve that represents the relationship between RhB concentration and absorbance.

To evaluate the practice applicability of APO, natural sunlight at noon (illuminance of 32766 lux) was used as an excitation source for the photocatalysis of the material. The steps are similar those of the above photocatalytic process using Xenon light.

3. Results and discussions

The crystal structure of as-synthesized samples was determined by X-ray diffraction (XRD) measurements. Fig. 1a shows XRD patterns of the products with different Ag^+/PO_4^{3-} ratios (3:1; 3:1.5; 3:2; 3:3) in precursor solutions. All patterns match well with JCPDS card No. 06-0505 with no strange peak, indicating that samples are pure Ag_3PO_4 with body-center cubic structure and space group P4-3n. The sharp peaks with small full-width half maxima (FWHM) of the peaks reveals that the samples were well crystallized. Through the positions and FWHM of reflection planes, the lattice parameters and the crystal diameter were calculated. The results show $a = b = c \sim 5.989$ Å and $D_{XRD} \sim 44$ nm for Ag/P 3:1 sample, which are relatively consistent with previous studies [4, 9, 12]. Fig. 1b depicts a comparison of the position of the sharp peak (210) between different samples which shows a shift towards a larger 2 theta angle as the Ag^+/PO_4^{3-} ratio decreases. This leads to a slight decrease in lattice parameters as shown in Table 1. In contrast to the decrease in lattice parameters, the crystal size increased which showed an increase in crystallinity as PO_4^{3-} content increases. This may be due to the high concentration of PO_4^{3-} inhibits the metallization of Ag^+ ions and stimulates the formation of crystal nuclei, which helps APO crystals to grow stronger.

Fig. 2 shows the scanning electron microscope (SEM) images of as-synthesized Ag_3PO_4 samples. All samples possess a spherical morphology with relatively uniform particle size. It is

obvious that the size of particles increases with increasing PO_4^{3-} content. The particle size distribution performed using ImageJ software showed that the average grain sizes of the samples were approximately 160 nm, 175 nm, 215 nm, and 230 nm for samples Ag/P 3:1, Ag/P 3:1.5, Ag/P 3:2, and Ag/P 3:3, respectively. This suggests that the excess PO_4^{3-} concentration not only stimulates crystal growth, but also promotes agglomeration of crystals to produce larger particles. It is a fact that if the concentration of PO_4^{3-} is low, the Ag^+ ions with a small radius meet each other with a higher probability, promoting metallization to Ag^o. Therefore, increasing the concentration of PO_4^{3-} would limit the metallization of Ag^+ and increase the probability of APO crystal nucleation, leading to faster growth of APO crystals, resulting in larger grain size.

Energy-dispersive X-ray spectroscopy EDX was used to analyze the element composition of as-synthesized samples. Fig. 3a shows that all peaks are consistent with the component elements of Ag_3PO_4 crystal as Ag, O and P. The results of the BET specific surface analysis performed through nitrogen adsorption-desorption measurements are presented in Fig. 3b and Table 1. Table 1 shows that the specific surface area of as-synthesized samples is quite small, only about 2-3 m^2/g, relatively consistent with previous reports [12, 25, 26]. Therefore, although Fig. 3b shows the separation of the adsorption and desorption curves, the difference in absolute quantitative adsorbed values between them is not significant. It is well known that the large surface area provides more active center for the photocatalytic activity, thereby increasing the photocatalytic efficiency. However, with this result, it can be predicted that the adsorption capacity of as-prepared sample is small, the photocatalytic efficiency is not brought about from the large surface area, but mainly relies on the photocatalytic activity of the material itself.

Fig. 4a presents FTIR spectra of prepared APO samples. It is obvious that all needed characteristic absorption bands of APO were depicted. The signal at 1635 cm^{-1} and 3435 cm^{-1} were attributed to the bending and stretching modes of adsorbed water molecules. The absorption peaks at 2350 cm^{-1} can be assigned to the asymmetric stretching mode (ν_3) of absorbed CO_2 the surface of APO [27]. The characteristic bands of PO_4 groups appeared at 560 cm^{-1} (antisymmetric bending mode ν_4) and 1015 cm^{-1} (antisymmetric stretching ν_3) [28, 29]. In addition, the band at 1390 cm^{-1} can be assigned to nitrate groups resulting from synthesis residuals. It can be said that the FTIR spectra have indirectly reflected the presence of components constituting the synthesized sample. A detail comparison of the FTIR peak position at 1015 cm^{-1} is presented in Fig. 4b. A small shift of the vibrational frequency towards higher wave numbers was observed as the PO_4^{3-} concentration increases, which is consistent with the slight decrease of lattice constant observed in the XRD results.

Raman spectra of the fabricated samples were performed to help detect small changes in the crystal lattice and shown in Fig. 5. In the wavenumber range of 100-1100 cm^{-1}, samples exhibited 5 Raman peaks at 223 cm^{-1}, 398 cm^{-1}, 551 cm^{-1}, 906 cm^{-1}, and 1064 cm^{-1}, most of them are low in intensity except the peak at 906 cm^{-1}. The low peak at 223 cm^{-1} was assigned to vibration mode (rotation or translation) of the tetrahedron [PO_4] while 398 cm^{-1} and 551 cm^{-1} peaks were the symmetric (E) and asymmetric (T_2) bending modes of [PO_4] cluster, respectively [30]. It is observed that the intense peak at 906 cm^{-1} is not only shifts towards the high wave number (902 cm^{-1} for Ag/P 3:1 sample and 906 cm^{-1} for Ag/P 3:3 sample) but also expands and becomes asymmetric as the Ag^+/PO_4^{3-} ratio decreases. Fig. 5b detailly depicts the peak at 906 cm^{-1} which shows that the 906 peak consists of three components of 906 cm^{-1}, 911 cm^{-1} and 972

cm^{-1}. They can be attributed to symmetric stretching vibration (A_1) and two asymmetric stretching modes (T_2) of [PO_4] group [30], respectively. The shift of 906 cm^{-1} peak is in an agreement with XRD and FTIR results, which both confirm the small deformation of crystal lattice upon Ag^+/PO_4^{3-} change in precursor solution.

X-ray photoelectron spectroscopy (XPS) measurements with the energy resolution of 0.1 eV were performed to investigate the composition of chemical elements on the surface of as-synthesized samples and to monitor the changes between their bonds (Fig. 6). The XPS spectra were calibrated with respect to the binding energy of the adventitious C 1s peak at 284.8 eV. Fig. 6a shows the survey XPS spectra for Ag/P 3:1 and Ag/P 3:1.5 samples which indicate the existence of all needed elements in the photocatalyst as Ag, P, and O. The appearance of the C 1s peak at 284.8 eV is due to the inherent presence of absorbed CO_2 molecules on the surface of the material or even originates from the adventitious hydrocarbon in the XPS instrument. The relevant high-resolution XPS spectra of the constituent elements Ag, O, and P is shown in Fig. 6b, c, and d, respectively. The peaks at binding energies of 367.6 eV and 373.6 eV were assigned to Ag $3d_{5/2}$ and Ag $3d_{3/2}$ state of which are characteristic for Ag^+ ions (Fig. 6b) [31]. Based on the asymmetry of the XPS peak, very small peaks at 369.5 eV and 375.4 eV were found which are believed corresponding to the metallization Ag^o state. The amount of metallization in both samples of Ag/P 3:1 and Ag/P 3:1.5 was evaluated by calculating the area ratio of the Ag^o and Ag^+ peaks. Table 2 shows that the Ag^o/Ag^+ ratio is above 3% for the Ag/P 3:1 sample and falls below 2% for the Ag/P 3:1.5 sample. This suggests that the metallization of Ag^+ ion decreases with increasing PO43- concentration to the excess level which is consistent with the aim of the study. Fig. 6c depicts XPS spectra of the O 1s state which includes some constituent peaks. The O1 peak at 530.2 eV could be assigned to O-Ag bonding while O2 peak at 532.2 eV is related to the dissociated OH group of H2O adsorbed on the Ag_3PO_4 surface [32]. Fig. 6d presents the high resolution XPS spectrum of the P 2p state of Ag/P 3:1 and Ag/P 3:1.5 samples. The spectrum includes 2 peaks at 132.5 eV and 134.0 eV for the P $2p_{3/2}$ state and P $2p_{1/2}$, respectively. These peaks shift towards the higher binding energies of 133.3 eV and 134.5 eV for Ag/P 3:1.5 sample which is likely due to the compression of the tetrahedron [PO_4] as shown in XRD, FTIR and Raman results.

The UV-vis absorption spectroscopy was performed to determine the optical absorption and energy bandgap of as-synthesized APO as shown in Fig. 7a. All samples exhibit strong absorption at wavelength shorter than 520 nm, demonstrating that visible radiation can be effectively used in the photoexcitation. Using the Kubelka-Munk function, the band gap E_g can be determined from the plot of $(\alpha hv)^{1/2}$ as a function of the photon energy (hc/λ) for indirect semiconductor as shown in Fig. 7b. The result shows that energy band gap is 2.43 eV which is in a good agreement with previous reports [31, 33]. As the PO_4^{3-} concentration increases, the absorbance for wavelengths less than 530 nm increases while the absorption background (above 530 nm) decreases. This is consistent with higher crystallinity as the PO_4^{3-} concentration increases as observed above.

Since the photoluminescence (PL) resulting from the recombination of the excited electrons and holes, the room temperature photoluminescence spectra were measured (excitation wavelength of 350 nm) to help evaluating the separation efficiency of photoexcited charge carriers in as-synthesized APO samples and shown in Fig. 8a. The results show that all APO

samples fluoresce in a wide range from 400 nm to 700 nm, with a strong emission peak around 520 nm (correspond to the band gap of 2.43 eV for APO material). It is observed that Ag/P 3:1 and Ag/P 3:1.5 samples possessed the weakest PL intensity, suggesting the lowest electron/hole recombination rate which is beneficial for the enhancement of photocatalytic activity. In addition, the normalized PL spectra in Fig. 8b show a shift of the PL emission peaks towards a larger wavelength as the ratio of Ag^+/PO_4^{3-} decreased, which was most pronounced for the Ag/P 3:2 sample.

The photocatalytic performance of the APO samples under visible light irradiation was evaluated through the decomposition of 10 ppm RhB without any additional sacrificial reagents using Xenon lamp illumination. Fig. 9a shows curves representing the relative C/C_o ratios of RhB in solution over time. Before light irradiation, the solutions were magnetically stirred in the dark for 30 min to achieved adsorption-desorption equilibrium. The results showed that the APO samples quickly reached the saturated adsorption state in less than 10 minutes with an adsorption rate of about 10% of the RhB concentration in the solution. The low RhB adsorption rate of the samples could be explained by the very low specific surface area as observed in the BET measurements. When illuminated, all the synthesized APO samples showed strong photocatalytic performance, completely decomposing RhB in less than 30 min, especially for the Ag/P 3:1.5 sample in only about 15 minutes. It is worth noting that the samples synthesized under PO_4^{3-} excess condition showed greater photocatalytic efficiency than the samples with the Ag^+/PO_4^{3-} ratio of 3:1. This can be explained by the high crystallinity of APO as observed in the XRD results and the low rate of electron-hole recombination as in the PL results. However, along with good crystallization, the samples fabricated in PO_4^{3-} excess solution also had a sharp increase in particle size as indicated in the SEM results which limited the photocatalytic efficiency due to the small specific surface area. As a result, the Ag/P 3:1.5 sample has the strongest photocatalytic activity because of both good crystallinity and small particle size.

The pseudo-first-order kinetic model is used to determine photocatalytic reaction rate, $ln(C_o/C) = kt$, where the rate constant k can be achieved from the slope of the linear relationship of the plot $ln(C_o/C) = kt$ versus reaction time (Fig. 9b). The catalysts exhibit the reaction rate constant k~0.228, 0.211, 0.200, 0.175 for Ag/P 3:1.5, Ag/P 3:3, Ag/P 3:2, and Ag/P 3:1, respectively. To assess the practical applicability of as-synthesized APO, the photocatalytic decomposition of RhB were performed under illumination of natural sunlight at noon (Fig. 9c). The samples exhibit excellent photocatalytic activity under sunlight. The sample with the highest photocatalytic efficiency is still Ag/P 3:1.5, which completely decomposes RhB dye in 60 minutes, and the sample with the lowest photocatalytic efficiency is still Ag/P 3:1, which decomposes over 90% RhB within 120 minutes. The order of samples with photocatalytic efficiency from strong to weak is similar to that of the photocatalysis test under Xenon lamp.

4. Conclusions

The spherical nanoparticle Ag_3PO_4 was successfully synthesized by a facile co-precipitation method with Ag^+/PO_4^{3-} ratio of 3:1, 3:1.5, 3:2, and 3:3. The excess concentration of PO_4^{3-} in the precursor solution reduces the lattice constant, increases the crystallinity and particle size, increases the photocatalytic activity of Ag_3PO_4 compared with that with the Ag^+/PO_4^{3-} ratio of 3:1. The Ag/P 3:1.5 sample exhibited the strongest photocatalytic activity due to its high

crystallinity, small particle size and lowest electron-hole recombination rate. The study shows the practical applicability of Ag_3PO_4 material for photocatalytic degradation of polluted organic substances in natural environment using sunlight.

Author contributions Methodology and experiment, Mai V.T., Hang L.T.; formal analysis, Hang L.T.; investigation, Chung P.D., Hung N.M., Thang D.V.; writing—original draft preparation, Oanh L.T.M.; writing—review and editing, Hung N.M., Oanh L.T.M., Chung P.D.; supervision, Minh N.V. All authors have read and agreed to the published version of the manuscript.

Funding: This work was supported by a scientific and technological project at the level of Ministry of Education and Training, grand number B2020-MDA-11.

References

1. Yi Z; Ye J; Kikugawa N; Kako T; Ouyang S; Stuart-Williams H; Yang H; Cao J; Luo W; Li Z; Liu Y; Withers R L, An orthophosphate semiconductor with photooxidation properties under visible-light irradiation 2010 *Nat. Mater* **9** (7) 559-64
2. Chen X; Dai Y; Wang X, Methods and mechanism for improvement of photocatalytic activity and stability of Ag3PO4: A review 2015 *J. Alloys Compd.* **649** 910-932
3. Deng J; Pang H; Deng D; Zhang J, Facile control synthesis of Ag3PO4 and morphologies effects on their photocatalytic properties 2012 *Proceedings of the Institution of Mechanical Engineers, Part N: Journal of Nanoengineering and Nanosystems* **225** (2) 67-69
4. Huang G-F; Ma Z-L; Huang W-Q; Tian Y; Jiao C; Yang Z-M; Wan Z; Pan A, Ag3PO4 Semiconductor Photocatalyst: Possibilities and Challenges 2013 *J. Nanomater.* **2013** 1-8
5. Batvandi M; Haghighatzadeh A; Mazinani B, Synthesis of Ag3PO4 microstructures with morphology-dependent optical and photocatalytic behaviors 2020 *Appl. Phys. A* **126** (7)
6. Dong P; Hao Y; Gao P; Cui E; Zhang Q, Synthesis and Photocatalytic Activity of Ag3PO4Triangular Prism 2015 *J. Nanomater.* **2015** 1-6
7. Amornpitoksuk P; Intarasuwan K; Suwanboon S; Baltrusaitis J, Effect of Phosphate Salts (Na3PO4, Na2HPO4, and NaH2PO4) on Ag3PO4 Morphology for Photocatalytic Dye Degradation under Visible Light and Toxicity of the Degraded Dye Products 2013 *Ind. Eng. Chem. Res.* **52** (49) 17369-17375
8. Dong L; Wang P; Wang S; Lei P; Wang Y, A simple way for Ag 3 PO 4 tetrahedron and tetrapod microcrystals with high visible-light-responsive activity 2014 *Mater. Lett.* **134** 158-161
9. Febiyanto F; Sulaeman U, The Starting Material Concentration Dependence of Ag3PO4 Synthesis for Rhodamine B Photodegradation under Visible Light Irradiation 2020 *Jurnal Kimia Valensi* **6** (1) 1-9
10. Afifah K; Andreas R; Hermawan D; Sulaeman U, Tuning the Morphology of Ag3PO4 Photocatalysts with an Elevated Concentration of KH2PO4 2019 *Bull. Chem. React. Eng. Catal.* **14** (3)
11. Yang Z-M; Liu Y-Y; Xu L; Huang G-F; Huang W-Q, Facile shape-controllable synthesis of Ag 3 PO 4 photocatalysts 2014 *Mater. Lett.* **133** 139-142
12. Guan X; Shi J; Guo L, Ag3PO4 photocatalyst: Hydrothermal preparation and enhanced O2 evolution under visible-light irradiation 2013 *Int. J. Hydrog. Energy* **38** (27) 11870-11877
13. Futihah I; Riapanitra A; Yin S; Sulaeman U, The pH dependence of Ag3PO4 synthesis on visible light photocatalytic activities 2020 *J. Phys. Conf. Ser. 1494*

14. Liu Q; Li N; Qiao Z; Li W; Wang L; Zhu S; Jing Z; Yan T, The Multiple Promotion Effects of Ammonium Phosphate-Modified Ag3PO4 on Photocatalytic Performance 2019 *Front. Chem.* **7** 866
15. Yan T; Guan W; Li W; You J, Ag3PO4photocatalysts loaded on uniform SiO2supports for efficient degradation of methyl orange under visible light irradiation 2014 *RSC Adv.* **4** (70)
16. Qin J; Zhang X; Yang C; Song A; Zhang B; Rajendran S; Ma M; Liu R, Effect of Ag+ and PO43− ratios on the microstructure and photocatalytic activity of Ag3PO4 2016 *Funct. Mater. Lett.* **09** (05)
17. Febiyanto F; Soleh A; Amal M S K; Afif M; Sewiji S; Riapanitra A; Sulaeman U, Facile Synthesis of Ag3PO4 Photocatalyst with Varied Ammonia Concentration and Its Photocatalytic Activities For Dye Removal 2019 *Bull. Chem. React. Eng. Catal.* **14** (1)
18. Liang Q; Shi Y; Ma W; Li Z; Yang X, Enhanced photocatalytic activity and structural stability by hybridizing Ag3PO4 nanospheres with graphene oxide sheets 2012 *Phys. Chem. Chem. Phys.* **14** (45) 15657-65
19. Liu M; Wang G; Xu P; Zhu Y; Li W, Construction of Ag3PO4/SnO2 Heterojunction on Carbon Cloth with Enhanced Visible Light Photocatalytic Degradation 2020 *Appl. Sci.* **10** (9)
20. Zhang M; Du H; Ji J; Li F; Lin Y C; Qin C; Zhang Z; Shen Y, Highly Efficient Ag3PO4/g-C3N4 Z-Scheme Photocatalyst for Its Enhanced Photocatalytic Performance in Degradation of Rhodamine B and Phenol 2021 *Molecules* **26** (7)
21. Osman N S; Sulaiman S N; Muhamad E N; Mukhair H; Tan S T; Abdullah A H, Synthesis of an Ag3PO4/Nb2O5 Photocatalyst for the Degradation of Dye 2021 *Catalysts* **11** (4)
22. Panthi G; Gyawali K R; Park M, Towards the Enhancement in Photocatalytic Performance of Ag3PO4 Nanoparticles through Sulfate Doping and Anchoring on Electrospun Nanofibers 2020 *Nanomaterials (Basel)* **10** (5)
23. Xie Y P; Wang G S, Visible light responsive porous Lanthanum-doped Ag3PO4 photocatalyst with high photocatalytic water oxidation activity 2014 *J. Colloid Interface Sci.* **430** 1-5
24. Shi L; Liang L; Ma J; Wang F; Sun J, Remarkably enhanced photocatalytic activity of ordered mesoporous carbon/g-C(3)N(4) composite photocatalysts under visible light 2014 *Dalton Trans.* **43** (19) 7236-44
25. Tseng C S; Wu T; Lin Y W, Facile Synthesis and Characterization of Ag(3)PO(4) Microparticles for Degradation of Organic Dyestuffs under White-Light Light-Emitting-Diode Irradiation 2018 *Materials (Basel)* **11** (5)
26. Zwara J; Grabowska E; Klimczuk T; Lisowski W; Zaleska-Medynska A, Shape-dependent enhanced photocatalytic effect under visible light of Ag3PO4 particles 2018 *J. Photochem. Photobiol. A: Chem.* **367** 240-252
27. Infrared Spectroscopy 2020 https://chem.libretexts.org/@go/page/1847
28. Aufort J; Lebon M; Gallet X; Ségalen L; Gervais C; Brouder C; Balan E, Macroscopic electrostatic effects in ATR-FTIR spectra of modern and archeological bones 2018 *American Mineralogist* **103** (2) 326-329
29. Destainville A; Champion E; Bernache-Assollant D; Laborde E, Synthesis, characterization and thermal behavior of apatitic tricalcium phosphate 2003 *Mater. Chem. Phys.* **80** (1) 269-277
30. Trench A B; Machado T R; Gouveia A F; Assis M; da Trindade L G; Santos C; Perrin A; Perrin C; Oliva M; Andrés J; Longo E, Connecting structural, optical, and electronic properties and photocatalytic activity of Ag3PO4:Mo complemented by DFT calculations 2018 *Appl. Catal. B: Environmental* **238** 198-211

31. Song L; Yang J; Zhang S, Enhanced photocatalytic activity of Ag 3 PO 4 photocatalyst via glucose-based carbonsphere modification 2017 *Chem. Eng. J.* **309** 222-229
32. Chong R; Cheng X; Wang B; Li D; Chang Z; Zhang L, Enhanced photocatalytic activity of Ag 3 PO 4 for oxygen evolution and Methylene blue degeneration: Effect of calcination temperature 2016 *Int. J. Hydrog. Energy* **41** (4) 2575-2582
33. Liu Y; Qian Q; Yi Z; Zhang L; Min F; Zhang M, Low-temperature synthesis of single-crystalline BiFeO3 using molten KCl–KBr salt 2013 *Ceram. Int.* **39** (7) 8513-8516

Table captions

Table 1 Lattice parameters, diameter of crystallite and nanoparticle and specific surface area of as-synthesized Ag_3PO_4 with different Ag^+/PO_4^{3-} ratio in precursor solution (Ag^+/PO_4^{3-} = 3:1, 3:1.5; 3:2; 3:3)

Samples	**Lattice parameters a=b=c** (Å)	**Diameter of crystallite D_{XRD}** (nm)	**Particle diameter D_{SEM}** (nm)	**Specific surface area** (m^2/g)
Ag/P 3:1	5.989	44	~160	2.8
Ag/P 3:1.5	5.968	48	~175	3.0
Ag/P 3:2	5.972	41	~215	1.8
Ag/P 3:3	5.968	49	~230	1.8

Table 2 The area ratio of the Ag^o and Ag^+ XPS peaks (Ag^o:Ag^+) for the two spin orbit Ag $3d_{1/2}$ and Ag $3d_{3/2}$ in Ag/P 3:1 and Ag/P 3:1.5 samples

Sample	**Area ratio Ag^o:Ag^+** (%)	
	Ag $3d_{1/2}$	**Ag $3d_{3/2}$**
Ag/P 3:1	3.4%	3.1%
Ag/P 3:1.5	1.9%	1.2%

Figure captions

Fig. 1 a) XRD pattern of as-synthesized Ag_3PO_4 with different Ag^+/PO_4^{3-} ratio in precursor solution (Ag^+/PO_4^{3-} = 3:1; 3:1.5; 3:2; 3:3) and b) a comparison of (210) peak position.

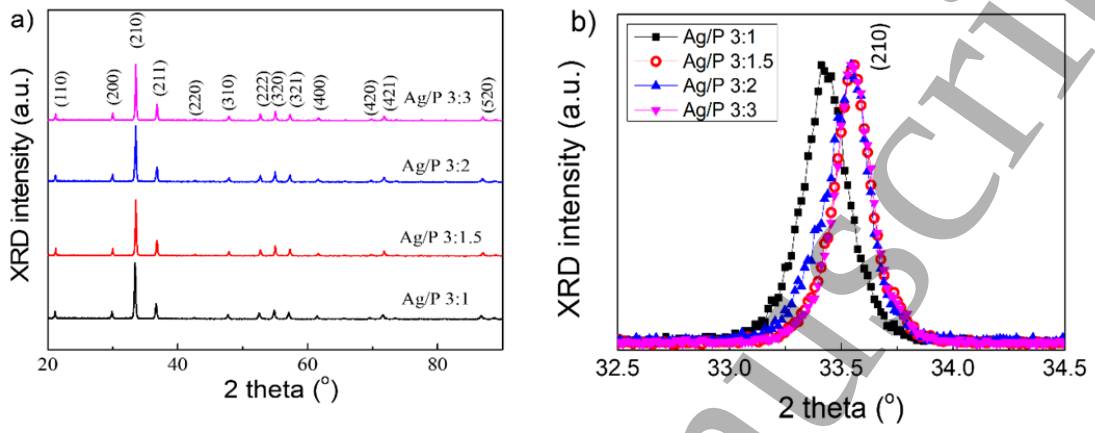

Fig. 2 SEM images of as-synthesized Ag_3PO_4 with different Ag^+/PO_4^{3-} ratio in precursor solution of a) 3:1, b) 3:1.5, c) 3:2, and d) 3:3

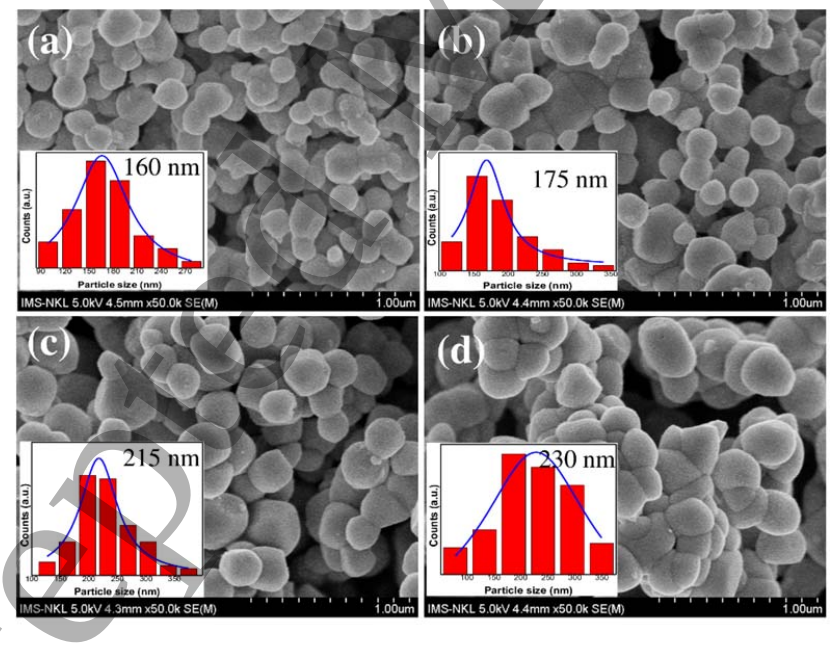

Fig. 3 a) EDX analysis and b) BET results of as-synthesized Ag_3PO_4 with different Ag^+/PO_4^{3-} ratio in precursor solution (Ag^+/PO_4^{3-} = 3:1; 3:1.5; 3:2; 3:3)

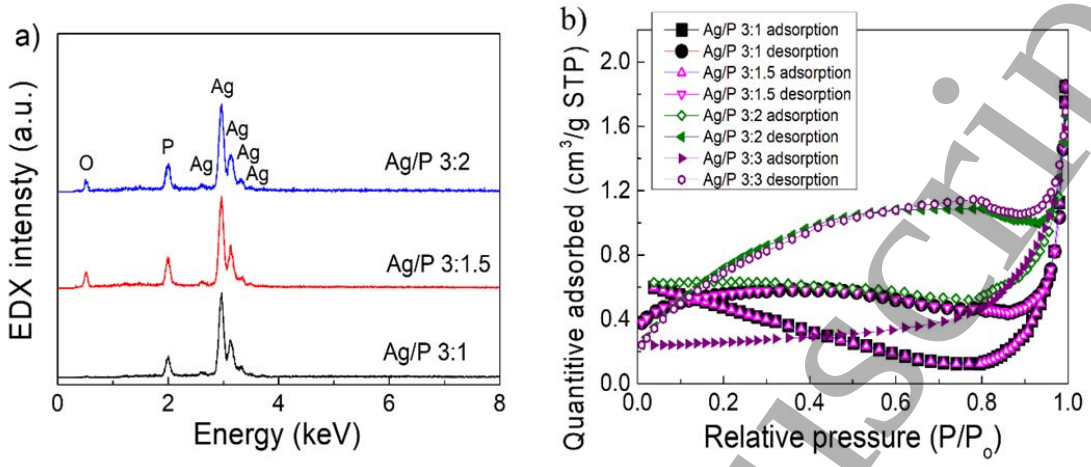

Fig. 4 a) FTIR spectra of as-synthesized Ag_3PO_4 with different Ag^+/PO_4^{3-} ratio in precursor solution (Ag^+/PO_4^{3-} = 3:1; 3:1.5; 3:2; 3:3) and b) a comparison of 1015 cm^{-1} peak position

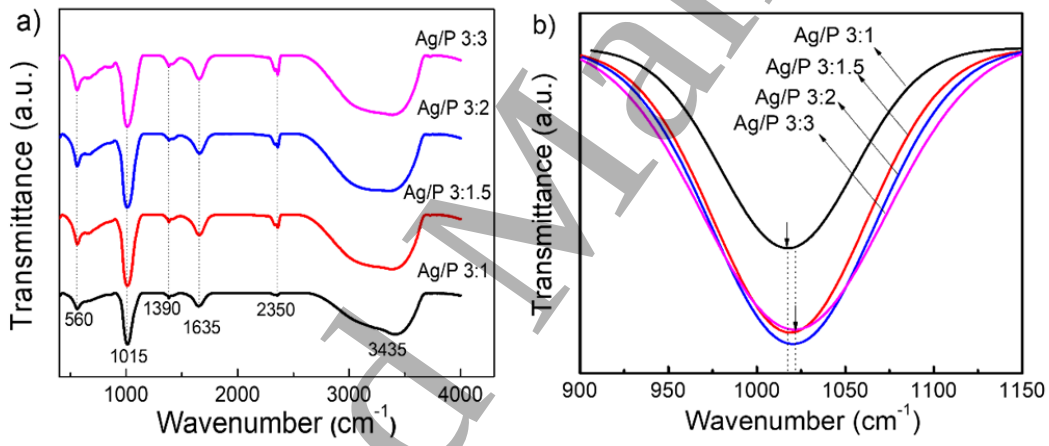

Fig. 5 a) Raman scattering spectra of as-synthesized Ag_3PO_4 with different Ag^+/PO_4^{3-} ratio in precursor solution (Ag^+/PO_4^{3-} = 3:1; 3:1.5; 3:2; 3:3) and b) a comparison of 906 cm^{-1} vibration peak

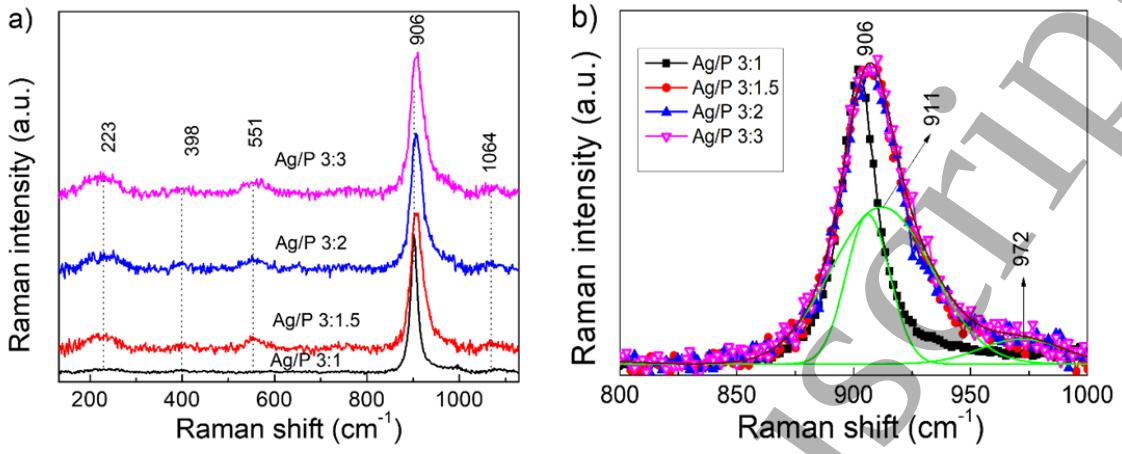

Fig. 6 a) XPS survey spectra of as-synthesized Ag_3PO_4 with different Ag^+/PO_4^{3-} ratio in precursor solution (Ag^+/PO_4^{3-} = 3:1; 3:1.5; 3:2; 3:3) and b) the relevant high-resolution XPS spectra of the constituent elements of b) Ag, c) O, and d) P

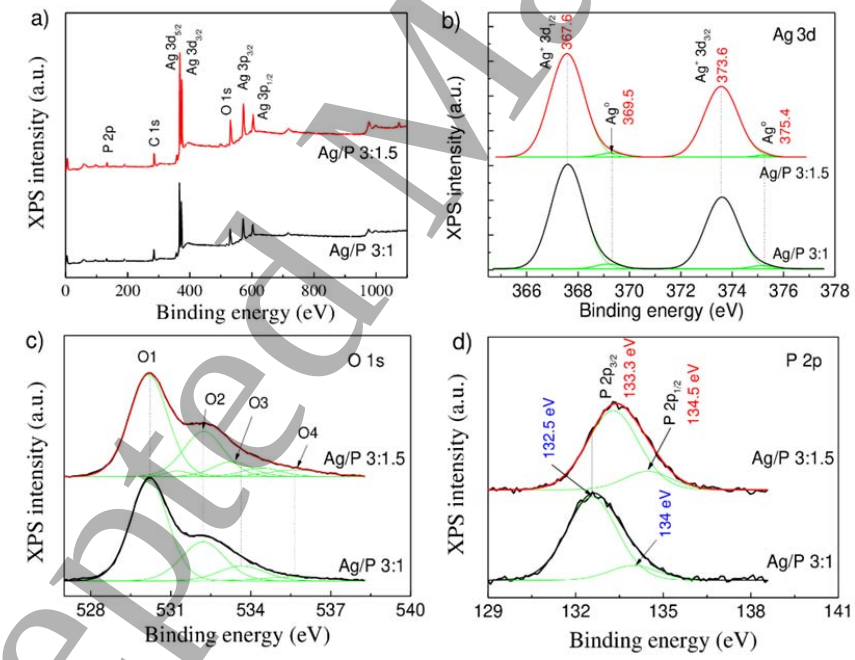

Fig. 7 a) UV-vis absorption spectra of as-synthesized Ag_3PO_4 with different Ag^+/PO_4^{3-} ratio in precursor solution (Ag^+/PO_4^{3-} = 3:1; 3:1.5; 3:2; 3:3) and b) the method to determine energy band gap from the plot of $(\alpha hv)^{1/2}$ versus photon energy hc/λ

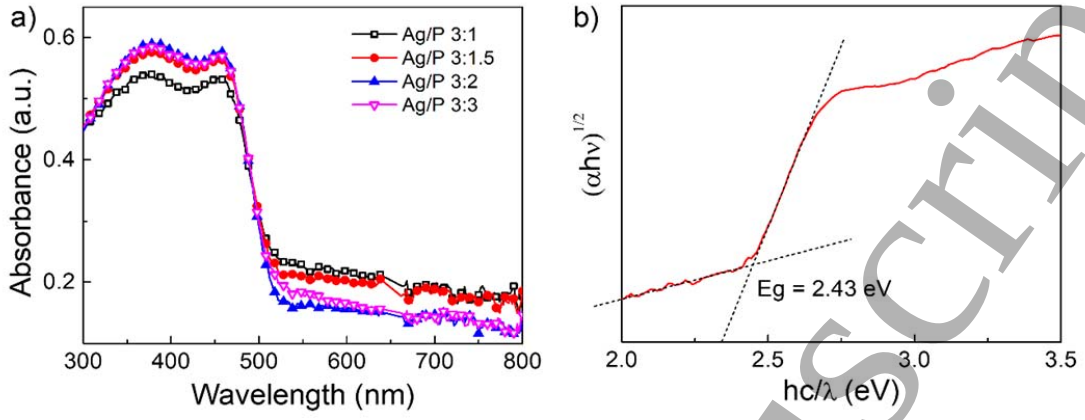

Fig. 8 a) PL spectra of as-synthesized Ag_3PO_4 with different Ag^+/PO_4^{3-} ratio in precursor solution (Ag^+/PO_4^{3-} = 3:1; 3:1.5; 3:2; 3:3) and b) the normalized PL spectra

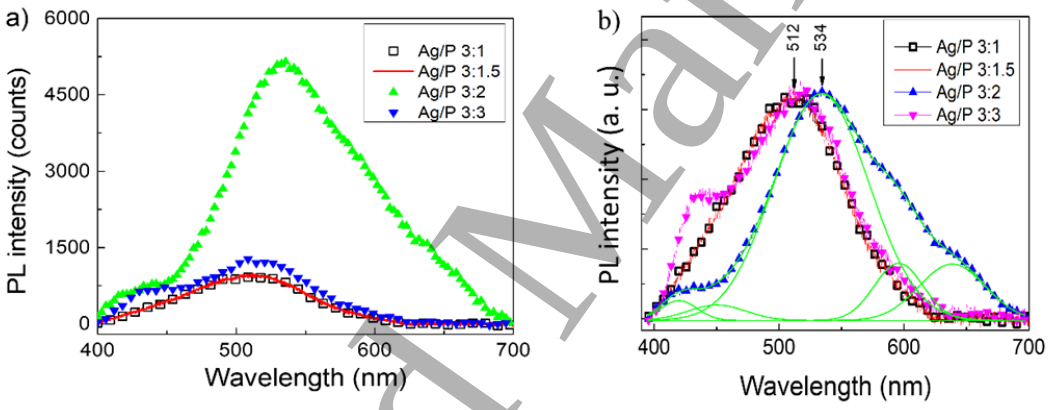

Fig. 9 a) Photocatalytic activities and b) reaction rate of as-synthesized Ag_3PO_4 in decomposing RhB solution under visible light using Xenon lamp; c) photocatalytic activities under natural sunlight